Geophysical Research Letters

RESEARCH LETTER
10.1029/2023GL107188

Improving Mercury Systematics With Molybdenum and Vanadium Enrichments: New Insights From the Cambrian-Ordovician Boundary

Leibo Bian[1,2], Anthony Chappaz[3], Xiaomei Wang[1], David Amouroux[4], Niels Hemmingsen Schovsbo[5], Xiaowei Zheng[6], and Hamed Sanei[2]

[1]Research Institute of Petroleum Exploration and Development, Beijing, China, [2]Department of Geoscience, Lithospheric Organic Carbon Group, Aarhus University, Aarhus, Denmark, [3]Department of Earth and Atmospheric Sciences, STARLAB, Central Michigan University, Mount Pleasant, MI, USA, [4]Université de Pau et des Pays de l'Adour, E2S/UPPA, CNRS, Institut des Sciences Analytiques et de Physico-chimie pour L'environnement et Les Matériaux, Pau, France, [5]Department of Geoenergy and Storage, Geological Survey of Denmark and Greenland, Copenhagen, Denmark, [6]State Key Laboratory of Petroleum Resources and Prospecting, China University of Petroleum, Beijing, China

Abstract The Cambro-Ordovician interval marks a significant transition from extinction to bio-diversification in deep time. However, the relationship of bio-transition to volcanism, commonly characterized by mercury (Hg) systematics in sedimentary records, has not been examined. We present the first Cambro-Ordovician Hg systematics from the Scandinavian Alum Shale. Our results show pronounced Furongian Hg enrichments, coupled with positive Δ^{199}Hg, Δ^{200}Hg, and Δ^{201}Hg values and negative Δ^{204}Hg values that we ascribe to atmospheric Hg transport over long-distances, while Early Ordovician Hg anomalies, characterized by near-zero mass-independent isotope values, indicative of submarine source. Our findings are supported by two new proxies: molybdenum-Hg and vanadium-δ^{202}Hg co-variations, demonstrating Hg systematics were strongly influenced by changes in source and depositional conditions. Constrained by a synchronous atmospheric-tectonic-oceanic model, we hypothesize Furongian subaerial volcanism contributed to global extinction and oceanic anoxia, whereas Early Ordovician submarine volcanism concurrent with ocean water upwelling promoted the nascent bio-diversification.

Plain Language Summary The late Cambrian-Early Ordovician interval is a crucial time that bridges the Cambrian extinction and Great Ordovician Bio-diversification events. The former is associated with 50% decrease in genera, whereas the latter displays threefold increase in species. Volcanism is associated with extinction and bio-development events throughout Earth's history. Prior works investigated potential biogeochemical controls that could have supported the Cambro-Ordovician bio-transition, but none explored the role of volcanism. We, for the first time, examine Hg abundance ratios and isotopes in the Scandinavian Alum Shale core across this boundary. Two novel molybdenum-Hg and vanadium-δ^{202}Hg models are proposed to improve our interpretation of the geochemical records about the effects of volcanism on environmental changes during this enigmatic transition. Constrained by a synchronous atmospheric-oceanic-tectonic model, our results demonstrate that late Cambrian subaerial volcanism contributed to oceanic anoxia and extinction, whereas Early Ordovician submarine volcanism and water upwelling led to the subsequent bio-radiation.

Key Points:

- Mercury is associated with organic matter in carbonaceous Alum shale deposited under sulfidic conditions
- Late Cambrian-Early Ordovician mercury was released by volcanism that also triggered major environmental change
- Mercury mass independent fractionation isotopes suggest late Cambrian subaerial volcanism but Early Ordovician submarine source

Supporting Information:

Supporting Information may be found in the online version of this article.

Correspondence to:

X. Wang and H. Sanei,
wxm01@petrochina.com.cn;
sanei@geo.au.dk

Citation:

Bian, L., Chappaz, A., Wang, X., Amouroux, D., Schovsbo, N. H., Zheng, X., & Sanei, H. (2024). Improving mercury systematics with molybdenum and vanadium enrichments: New insights from the Cambrian-Ordovician boundary. *Geophysical Research Letters*, *51*, e2023GL107188. https://doi.org/10.1029/2023GL107188

Received 7 NOV 2023
Accepted 11 MAR 2024

Author Contributions:

Conceptualization: Leibo Bian, Anthony Chappaz
Data curation: Leibo Bian
Formal analysis: Leibo Bian, Anthony Chappaz, Xiaomei Wang, David Amouroux, Niels Hemmingsen Schovsbo, Xiaowei Zheng, Hamed Sanei
Funding acquisition: Xiaomei Wang, Hamed Sanei
Investigation: Leibo Bian, Niels Hemmingsen Schovsbo

1. Introduction

The late Cambrian-Early Ordovician interval is a significant time in Earth's history because it connected two crucial lower Paleozoic evolutionary milestones: the late Cambrian extinction and the onset of Great Ordovician Bio-diversification Events (GOBE; Fan et al., 2020; Harper et al., 2020). The late Cambrian extinction witnessed several biological events that contributed to ~50% extinction rate of genera (Saltzman et al., 2015). The early Furongian extinction event, contemporaneous with the Steptoean Positive Carbon Isotope Excursion (SPICE) event, was mainly attributed to widespread oceanic anoxia with combined effects of thermal anomaly, polar wander events, and low nutrient input (Bian et al., 2023; Gill et al., 2011). Subsequent volcanic activity identified by anomalous Hg enrichments were likely responsible for the mid-Furongian recurrent extinction (Bian, Chappaz, Schovsbo, Nielsen, & Sanei, 2022). The Early Ordovician is seen as a preliminary biotic development of the GOBE that displays around a threefold increase in species diversity (Harper et al., 2020; Servais & Harper, 2018).

Methodology: Leibo Bian, Anthony Chappaz, David Amouroux, Xiaowei Zheng, Hamed Sanei
Project administration: Xiaomei Wang, Hamed Sanei
Resources: Leibo Bian
Software: Leibo Bian
Supervision: Anthony Chappaz, Xiaomei Wang, Niels Hemmingsen Schovsbo, Hamed Sanei
Validation: Leibo Bian, Anthony Chappaz, Xiaomei Wang, Niels Hemmingsen Schovsbo, Xiaowei Zheng, Hamed Sanei
Visualization: Leibo Bian, Anthony Chappaz, Xiaomei Wang
Writing – original draft: Leibo Bian, Anthony Chappaz, Xiaomei Wang, Hamed Sanei
Writing – review & editing: Leibo Bian, Anthony Chappaz, Xiaomei Wang, David Amouroux, Niels Hemmingsen Schovsbo, Hamed Sanei

Volcanism is an Earth's modulation mechanism that can induce atmospheric, terrestrial, and oceanic changes (Black et al., 2021), leading to either biological proliferation (Longman et al., 2021) or extinction (Lindström et al., 2019). Massive volcanism may trigger biological calamity, whereas gentle volcanism might promote an increase in biodiversity (Jones & Gislason, 2008). Anomalous Hg enrichments in sedimentary rocks, characterized by Hg abundance and isotope ratios, have been widely used to identify ancient volcanic eruptions (Sanei et al., 2012; Shen et al., 2022). Mercury isotopes display mass-dependent fractionation (MDF) denoted as δ^{202}Hg and mass-independent fractionations (MIF) denoted as Δ^{x}Hg (x is 199, 200, 201, and 204; Blum et al., 2014). They can provide insights into tracking Hg sources and identifying the processes involved during transport (Zerkle et al., 2020). The MDF is influenced by biotic and abiotic processes, but MIFs are solely affected by photochemical reactions through variations in magnetic isotope effect and nuclear self-shielding (Blum et al., 2014). Mercury isotopic signatures within sedimentary rocks not exhibiting MIF excursions are commonly attributed to magmatic sources (i.e., no exposure to photons; MIF = ∼0‰, Grasby et al., 2017) and the rapid erosion and fast particle settling of Hg phases (Meixnerová et al., 2021). Prior to the proliferation of terrestrial life, Hg disturbance in the biosphere occurred mainly via either direct deposition of Hg particles—tuff and volcanic ash layers in sedimentary rocks close to the volcano—or long-range global transport of gaseous Hg that was later oxidized as Hg(II) and was deposited through rainfall. This latter process produces positive Δ^{199}Hg, Δ^{200}Hg, and Δ^{201}Hg along with negative Δ^{204}Hg values (Blum & Johnson, 2017; Shen et al., 2022).

Across Earth's history, intensive volcanism activity has been associated with significant environmental and biological changes. However, no prior work has examined the impact of volcanism on biogeochemical cycles during the Cambro-Ordovician transition. This omission hinders a comprehensive understanding of environmental factors driving the transition from extinction to bio-diversification. Therefore, our objectives were (a) to identify Hg anomalies across the Cambro-Ordovician boundary by examining the Scandinavian Alum Shale, (b) to improve the use of Hg systematics by enhancing our interpretation with molybdenum (Mo) and vanadium (V) enrichments, and (c) to apply our new model to refine understanding of the relationship between environmental changes and volcanism. By integrating our new approach with a model that combines contemporaneous atmospheric-oceanic-biological changes, we provide new insights into the effects of volcanism on environment-life shifts across the Cambro-Ordovician boundary.

2. Materials and Methods

The Alum Shale Formation covers ∼1, 000, 000 km^2 in the western margin of Baltica and was deposited across the Miaolingian, Furongian, and Early Ordovician (Figure 1c; Nielsen & Schovsbo, 2015). It provides an excellent set-up for characterizing the Cambro-Ordovician environmental and biological changes, because of the constant connection to the Iapetus Ocean, enabling it to reflect global environmental fluctuations (Bian et al., 2023; Gill et al., 2011). Herein, we examine two Alum Shale cores: the Ottenby-2 core (GPS coordinates: 56.14741°N, 16.24433°E) and the DBH 15/73 core (GPS coordinates: 58.24190°N, 13.46498°E). The detailed description of the two cores are present in Supporting Information S1. Briefly, the deposition of Ottenby-2 core spans from the Miaolingian to Early Ordovician, whereas the DBH 15/73 core is from the Miaolingian to Furongian (Figure 2). They are predominately composed of organic-rich shales deposited in a shallow water depth.

A total of 205 samples were grounded by a corundum mortar and separated into several aliquots for the following measurements. Bulk elements were analyzed through an Inductively Coupled Plasma Mass Spectrometry (ICP-MS) at the Bureau Veritas Ltd., Vancouver, Canada. Total sulfur (TS) was determined by the CS 200 Analyzer at the Geological Survey of Denmark and Greenland, Denmark. For the DBH 15/73 core, sequential extraction of Hg was conducted, and Hg concentrations and speciation were analyzed by a AMA 254 Advanced Mercury Analyzer and/or the double species-specific spike isotope-dilution analysis together with Gas Chromatography-ICP-MS at the Institute of Analytical Sciences and Physical Chemistry for the Environment and Materials (IPREM), France. For the Ottenby-2 core, Hg contents were determined by a DMA-80 automatic Hg Analyzer (Milestone, Italy) and isotopes by a Cold Vapor Multicollector ICP-MS (Nu. Instrument U.K.) at the State Key Laboratory of Environmental Geochemistry, China. Further description about experimental procedures and analytical precision are available in Text S2 in Supporting Information S1.

The Chemical Index of Alteration was used to characterize weathering intensity (Text S2.5 in Supporting Information S1). Briefly, the CIA value is defined by the equation: $CIA = [Al_2O_3/(Al_2O_3 + CaO^* + Na_2O + K_2O)] \times 100$

10.1029/2023GL107188

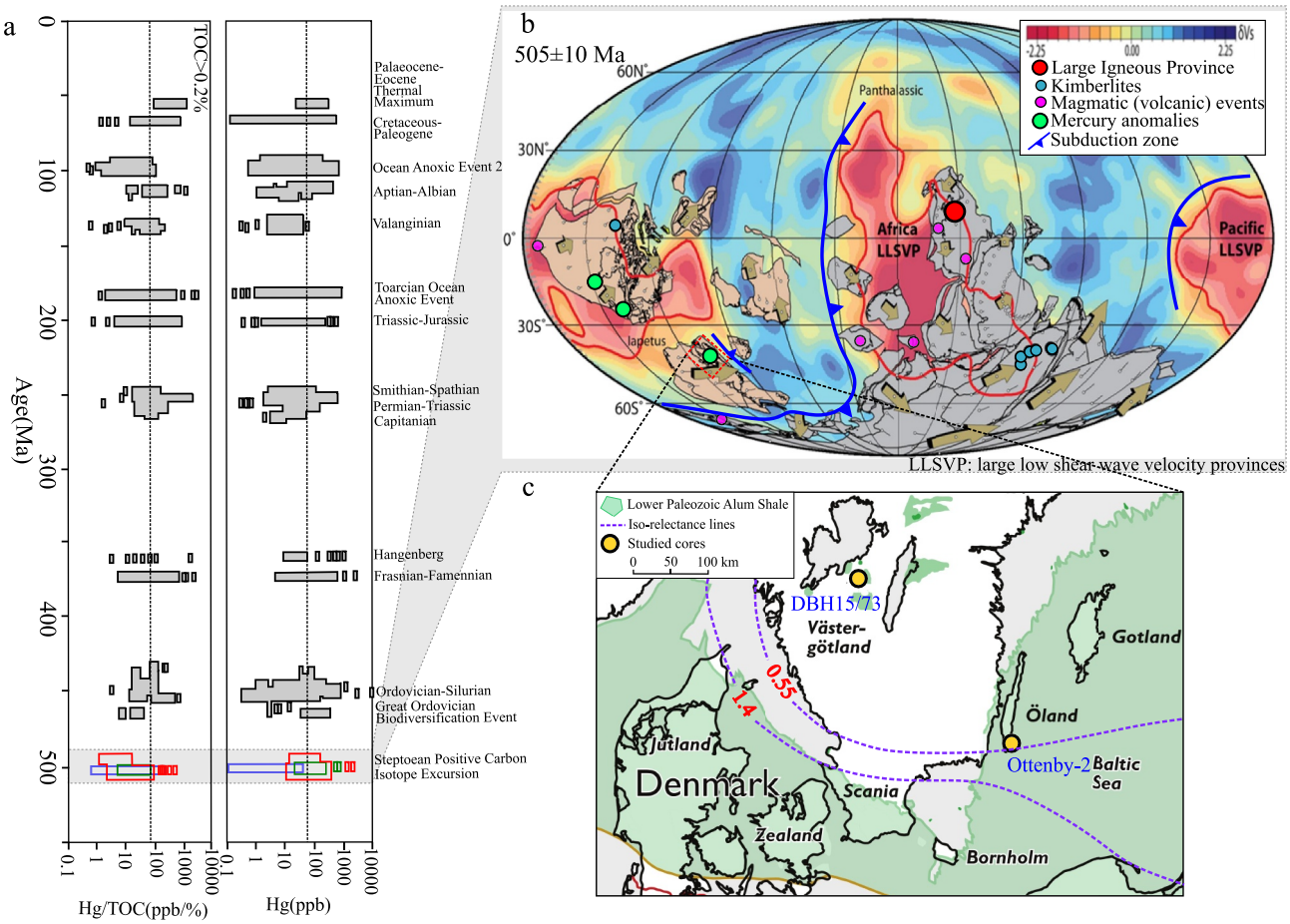

Figure 1. (a) Summary of mercury (Hg) concentrations in deep time (modified from Grasby et al., 2019); (b) Late Cambrian global reconstruction (Torsvik & Cocks, 2013), reported magmatic activity events, and Hg anomalies (Bian, Chappaz, Schovsbo, Nielsen, & Sanei, 2022; Hagen et al., 2022). (c) Locations of the Alum Shale cores and the thermal iso-reflectance line indicating the thermal maturity.

(Nesbitt & Young, 1982). The CaO* represents Ca in silicate-associated minerals and is calculated by the equation: CaO* = molar CaO–molar $P_2O_5 \times 10/3$. If the CaO* content is lower than the Na_2O content, the CaO* content is used. Otherwise, we use the Na_2O content to replace the originally calculated CaO* content (Chen et al., 2020; McLennan et al., 1993). In addition, all the correlations herein are characterized by the Spearman correlation coefficient (r_s; Hauke & Kossowski, 2011).

3. Results

3.1. The Chemo-Stratigraphy of the Ottenby-2 Core

Bian, Chappaz, Schovsbo, Nielsen, and Sanei (2022) identified four Hg anomalies during the late Cambrian based on Hg abundance ratios, Δ^{199}Hg, Δ^{200}Hg, and Δ^{201}Hg. The most pronounced Hg anomaly was observed after the SPICE event (Hg loading event III). Herein, we emphasize the description of the other data set.

In the Early Ordovician, several noticeable Hg enrichments (>150 ppb) are present from 12.8 to 8.8 m (loading event V; Figure 2b). Several Hg/TOC and Hg/TS peaks are also found (Figures 2c and 2d). Toward the top of this section, the trend does not have any particular pattern. The Δ^{199}Hg values remain around 0 ± 0.02‰ between 13.8 and 10.2 m, and then increase to 0.04‰. The Δ^{201}Hg values range from −0.01 to 0.03‰. The Δ^{200}Hg values remain ~0.01‰ from 12.4 to 9.4 m, and stay above 0.02‰ from 8.6 to 3.8 m (Figure 2).

10.1029/2023GL107188

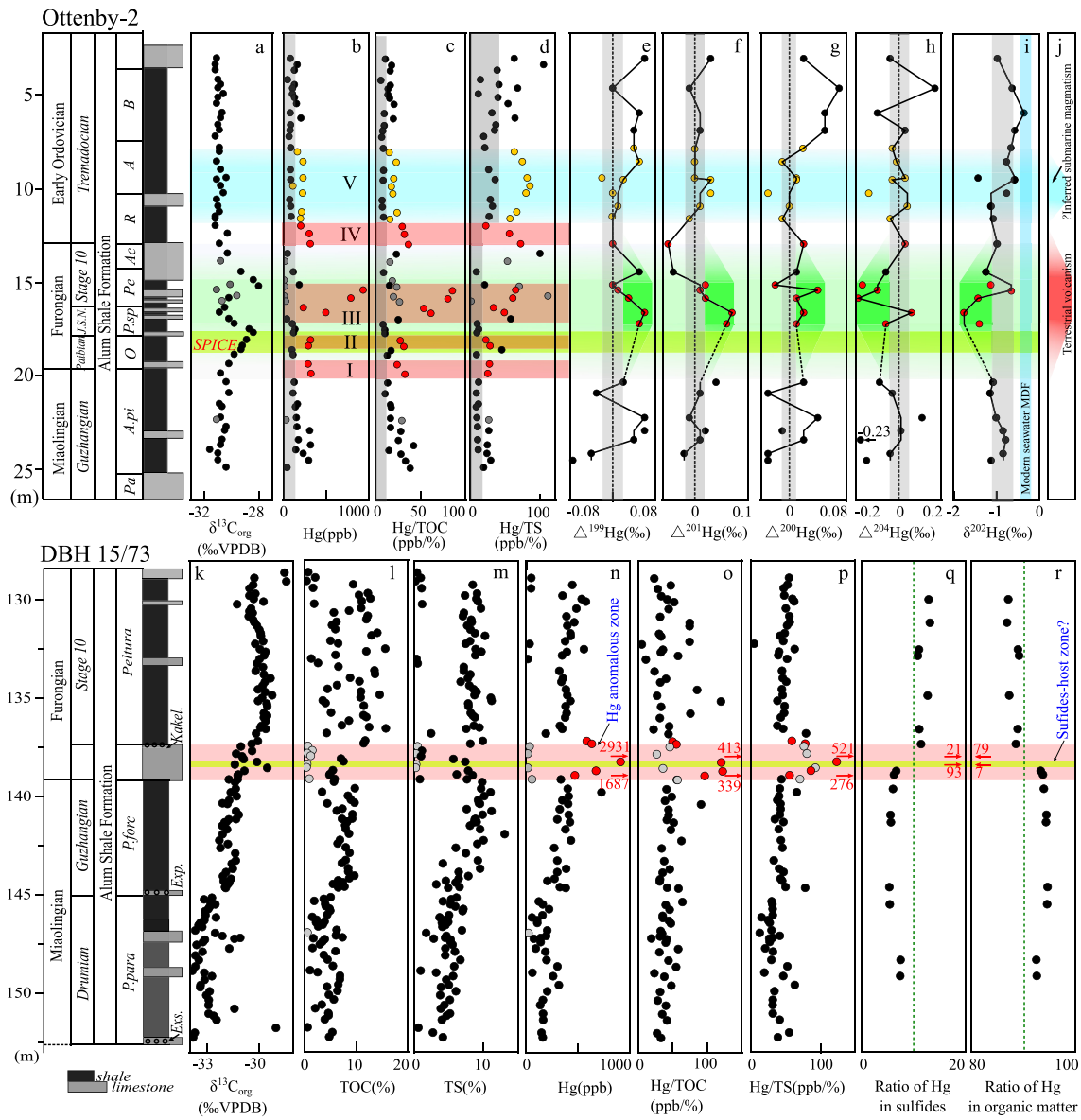

Figure 2. Profiles showing $\delta^{13}C_{org}$ and Hg systematics along with the litho- and bio-stratigraphy in Ottenby-2 (Panels a–j) and DBH (Panels k–r) cores. Within the bio-stratigraphy, *Pa*: *Paradoxides*; *A.pi*: *Agnostus pisiformis*; *O*: *Olenus*; *P.sp*: *Parabolina spinulosa*; *Pe*: *Peltura*; *Ac.*: *Acerocare*; *R*: *Rhabdinopora*; *A*: *Adelograptus tenellus*; *B*: *Brygraptus/Kiaerograptus*; *P.para.*: *Paradoxides paradoxissimus*; *P. forc.*: *Paradoxides forchammeri*. In the litho-stratigraphy, Kakel.: Kakelled Limestone Bed; Exp.: Exporrecta conglomerate; Exs.: Exsulans Limestone Bed-equivalent. Panels (a–p): gray circles represent organic-lean samples (TOC<1 wt%), yellow circles represent Ordovician Hg-anomalous samples, and red circles are late Cambrian Hg-anomalous samples; Panels (b–d): gray zones indicate the baseline values; Panels (e–i): gray zones represent no distinct Hg isotopic fractionations; Panels (n–r): the arrows with number indicate the values are beyond or below the threshold. TS: total sulfur; TOC: total organic carbon; SPICE: Steptoean Positive Carbon Isotope Excursion.

The Δ^{204}Hg values vary between −0.23 and 0.11‰ during the Miaolingian and are between −0.1 and 0.17‰ from 8.6 to 3.8 m (Figure 2h). Across Hg loading event III, the Δ^{204}Hg values range from −0.19‰ to −0.06‰, whereas the Δ^{204}Hg values are within ±0.04‰ during loading event V.

During the Miaolingian, the δ^{202}Hg values increase from −1.12‰ at 25.4 m to −0.79‰ at 24.3 m and then decrease to −1.15‰ at 21.1 m (Figure 2i). During loading event III, the δ^{202}Hg values show a positive excursion toward −0.66‰ and then stay −1.1‰ from 16.0 to 11.8 m. Toward the top of the core, the δ^{202}Hg values remain above −0.8‰ from 11.1 to 3.8 m.

3.2. The Chemostratigraphy of the DBH 15/73 Core

Total sulfur (TS) content remains around 5% throughout the Drumian (Figure 2m) and subsequently rises toward ~10% within the Guzhangian. During the early mid Furongian, the TS content diminishes to ~5% in organic-rich (TOC > 1%) shale samples and remains ~8% within the latest Furongian (Stage 10).

Mercury concentration ranges from 135 to 315 ppb during the Drumian (Figure 2n), followed by an increase from ~200 to ~400 ppb. During the early mid Furongian, Hg content in organic-rich shale samples rises up to ~2,930 ppb, followed by a decrease toward ~500 ppb, while the Hg content is relatively low in organic-lean (TOC ≤ 1%) samples. During the Stage 10, Hg content varies between ~300 and ~600 ppb.

The Hg/TOC ratio ranges from 30 to 50 ppb/% during the Miaolingian and late Furongian (Figure 2o). During the early mid Furongian, the Hg/TOC ratio in organic-rich shale samples gradually increases to ~120 ppb/%, followed by a decrease to ~50 ppb/%. The Hg/TS ratio is ~30 ppb/% in the Drumian and ~40 ppb/% in the Guzhangian (Figure 2p). During the early mid Furongian, the Hg/TS ratio in organic-rich and -lean samples reaches a maximum of ~100 ppb/%, and averages ~50 ppb/% during the late Furongian.

The ratio of Hg in sulfides accounts for ~6% in the Miaolingian, whereas it exceeds 10% in the Furongian (Figure 2q). The Hg percentage in organic matter ranges from ~93% to ~95% in the Miaolingian, whereas it oscillates between ~87% and ~89% during the Furongian (Figure 2r).

4. Discussion

4.1. Geochemical Controls Involved During the Burial of Mercury

Mercury is commonly associated with iron sulfide phases (as Hg-S species) and organic matter (as Hg(II)-thiol complexes and methyl Hg) in organic-rich sediments (Rickard & Morse, 2005; Shen et al., 2020). For the DBH 15/73 core, the results of Hg sequential extraction show that Hg in organic matter accounts for >80% of total Hg and in sulfides represent <20% (Figures 2q-r). This is consistent with previous studies, showing that Hg in organic-rich modern sediments is primarily bound to organic matter and subordinately to other compounds (i.e., sulfides) due to the high affinity of Hg (II) for organic matter (Fitzgerald et al., 2007; Wallace, 1982). We also observe that the Hg ratio in sulfides increases from the Miaolingian to Furongian. This could be attributed to the fact that sulfides play an increasing role in sequestrating Hg as sulfidic conditions became intense (Shen et al., 2019, 2020) or organic matter became depleted in the water column (Sanei et al., 2012).

The Hg-TOC and Hg-TS correlations are also investigated for host phases of Hg. In the late Cambrian, Hg exhibits a significant correlation with TOC in the Ottenby-2 core ($r_s = 0.74$, $p < 0.05$, $n = 24$; Figure S5c in Supporting Information S1). For the Miaolingian part of DBH 15/73 core, the significant correlation was determined ($r_s = 0.81$, $p < 0.05$, $n = 44$) but for the Furongian part, no statistical Hg-TOC correlation was found (Figure S5a in Supporting Information S1). Moreover, Hg and TS are significantly correlated in the late Cambrian ($r_s = 0.88$ ($p < 0.05$, $n = 72$) for the DBH core and $r_s = 0.93$ ($p < 0.05$, $n = 22$) for the Ottenby-2 core; Figures S5b and S5d in Supporting Information S1). Provided that organic matter is the primary host phases for Hg, we suggest the insignificant Hg-TOC correlation for the Furongian part of DBH15/73 core is attributed to different Hg and TOC burial rates. We infer that Hg is mostly associated with organic matter as Hg(II) complexed with organic thiols groups and/or with inorganic sulfides in a metacinnabar-like phases under sulfidic, organic-rich conditions (Graham et al., 2017; Skyllberg & Drott, 2010; Wolfenden et al., 2005). These two molecular structures are somehow similar to those of Mo and V that are present in organic matter through forming Mo-S and V-S species (Bian, Chappaz, Schovsbo, & Sanei, 2022; Chappaz et al., 2014).

Figures S5c-d show that Hg is insignificantly correlated to TOC and TS in the Early Ordovician samples ($p > 0.05$, $n = 21$). Because the redox conditions changed from extremely sulfidic conditions in the Furongian to intermediately sulfidic conditions in the Early Ordovician (Bian et al., 2023) and the TOC content remains above ~6% (Figure S5c in Supporting Information S1), we argue that organic matter and sulfides are major hosts for Hg, and infer that the insignificant relationship is ascribed to the Hg undersupply that led to apparently lower sequestration capability of the two host phases.

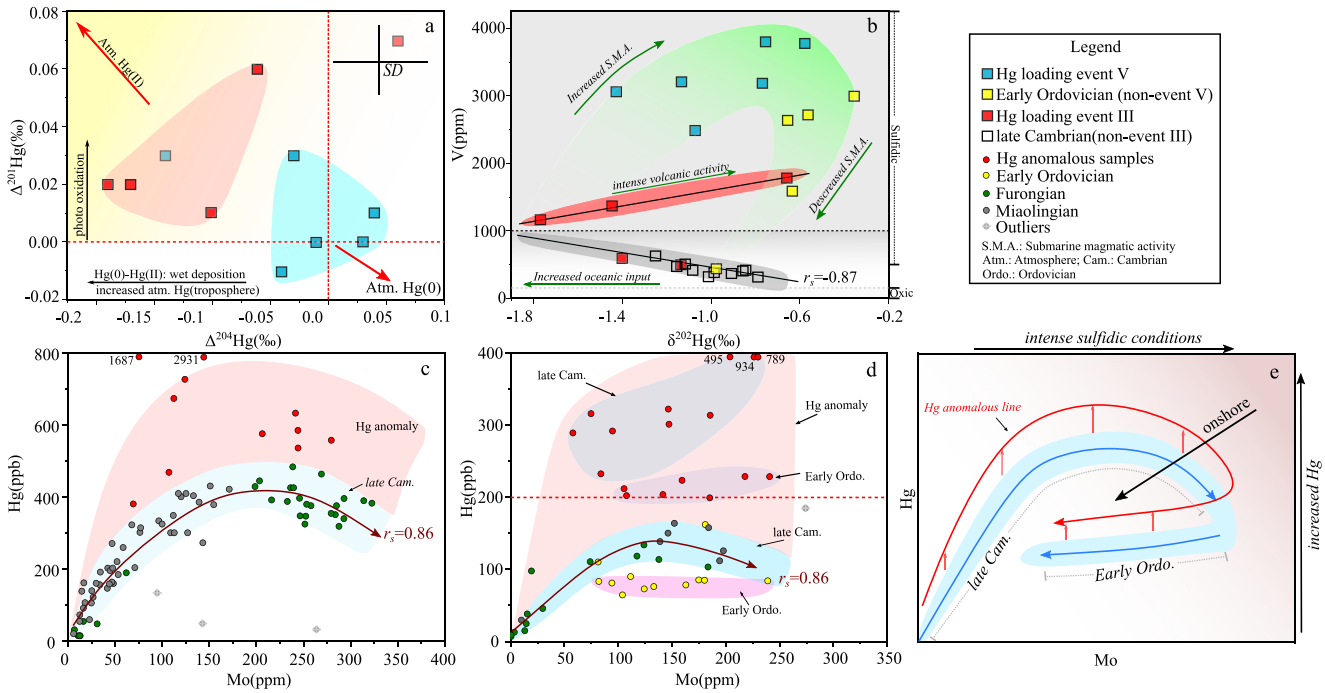

Figure 3. (a) Δ^{201}Hg versus Δ^{204}Hg values; (b) Vanadium versus δ^{202}Hg values; Molybdenum versus Hg in DBH 15/73 (c) and Ottenby-2 cores (d) as well as proposed model (e). Panel (b): $p < 0.05$, $n = 11$; Panel (c): $p < 0.05$, $n = 73$; Panel (d): $p < 0.05$, $n = 20$. Panels (b–d): For red circles with numbers, these numbers represent real Hg contents.

4.2. Contrasted Cambrian-Ordovician Hg Anomalies

Volcanism in sedimentary settings is associated with enrichments of Hg (i.e., anomalies) (Grasby et al., 2019). Herein, we focus mainly on interpreting Hg loading events III and V (Figure 3a; Supporting Information S1), because (a) they display the most pronounced and intense Hg abundances and therefore may alleviate the possible interferences from terrestrial fractions (Figure 2); (b) the strata hosting Hg anomalies are composed of felsic igneous rocks, suggesting minimal change and influence of provenance (Figure S6 in Supporting Information S1); and (c) the Chemical Index of Alteration (CIA) remains stable (Figure S1i in Supporting Information S1), which rules out the influence of enhanced terrestrial erosion that transported excess Hg sources.

During loading event III, positive but continuously decreasing Δ^{199}Hg and Δ^{201}Hg values along with slightly positive Δ^{200}Hg values were reported by Bian, Chappaz, Schovsbo, Nielsen, and Sanei (2022). The negative Δ^{204}Hg ($-0.19‰ \sim -0.06‰$) and positive Δ^{201}Hg values ($0.01‰ \sim 0.07‰$) indicate Hg was exposed to photons and deposited via rainfall (Figure 3a; Demers et al., 2013; Blum & Johnson, 2017). These data suggest Hg was transported in the atmosphere over long distances before being sequestrated in sediments (Figure 4g). Mercury loading event V exhibits Δ^{204}Hg values within $\pm 0.04‰$ and Δ^{199}Hg, Δ^{200}Hg, Δ^{201}Hg values close to zero, supporting a scenario where Hg was not exposed to photons (i.e., submarine volcanism; Figure 3a and Figure S8 in Supporting Information S1). We thus argue that subaerial volcanism contributed to the late Cambrian Hg enrichments whereas submarine volcanic activity occurred in the Early Ordovician.

4.3. The Covariation of Hg Systematics With Mo and V

4.3.1. The Mo-Hg Proxy

The residence time of Hg is less than ~2 years in the atmosphere and can be used to represent the transient variation of Hg flux in Earth's history (Mason & Sheu, 2002; Selin, 2009), whereas Mo displays a long residence time in the ocean water (~400 kyr; Miller et al., 2011). Provided that Hg and Mo are preferentially buried with organic matter and iron sulfide phases (Chappaz et al., 2018; Hlohowskyj et al., 2021; Shen et al., 2020), we propose to use the Hg-Mo relationship as a tool to refine our understanding of Hg sequestration under reducing

10.1029/2023GL107188

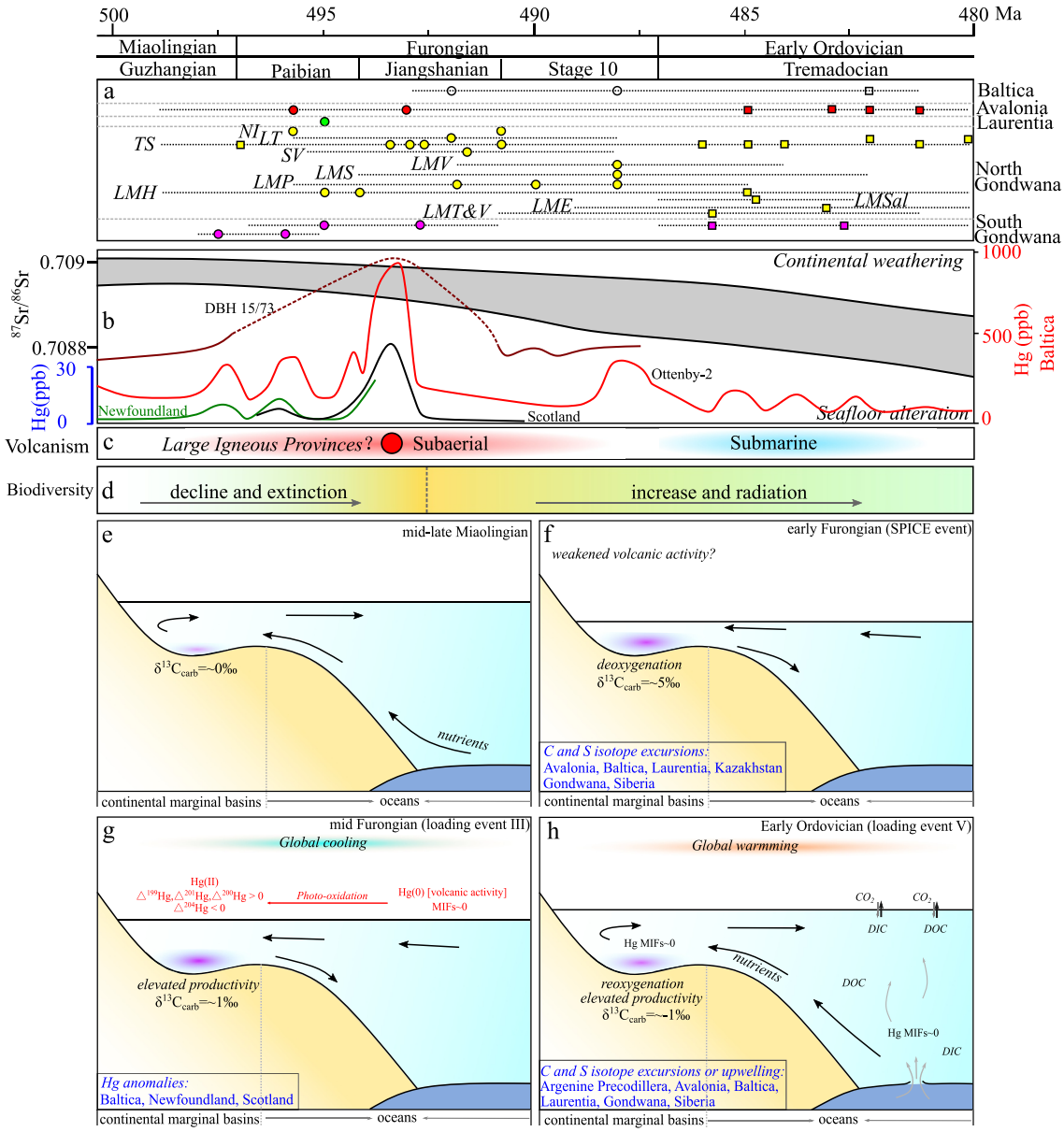

Figure 4. (a) A summary of synchronous magmatic activity. The dots were previously collected in Bian, Chappaz, Schovsbo, Nielsen, and Sanei (2022) and the squares are collected (Table S1 in Supporting Information S1); (b) the gray area is strontium isotope data ($\delta^{87}Sr/^{86}Sr$, McArthur et al., 2020) and reported Hg concentrations in sedimentary records. (c) Inferred global volcanism; (d) the changes in biodiversity; (e)–(f): global environmental variations in continental margin basins and oceans. In (e–f), the lower lefthand corners include the globally reported synchronous environmental variations, the area changing from purple to blue represents oxygen minimum zone. Further details refer to Figure S10 in Supporting Information S1.

conditions. By investigating the Hg-Mo relationship, we aim to constrain the transient Hg abundance variations in seawater, not to identify the host phases.

Not accounting for the samples showing anomalies ($n = 15$, Figure 3c; $n = 11$, Figure 3d), Hg displays a high correlation with Mo ($r_s = 0.86$, $p < 0.05$, $n = 73$, Figure 3c; $r_s = 0.86$, $p < 0.05$, $n = 20$, Figure 3d). For the DBH 15/73 core deposited under a deeper water column, Hg is positively correlated with Mo during the Miaolingian, but shows a negative relationship with Mo during the Stage 10 (Figure 3c). We assume the Hg/Mo ratio remains stable for anomaly free horizons (Meixnerová et al., 2021). Consequently, we propose the Hg enrichments result from a constant Hg supply and that the inversed relationship represents a transient increase before loading event III followed by a decrease in Hg supply.

During the Tremadocian, we focus on the lower part for two reasons: (a) the high level (>200 ppb) of Hg and (b) a limited Hg isotope data set for the upper part. Figure 3d shows that Hg remains ~90 ppb whilst Mo varies from 80 to 200 ppm. Because the Hg enrichments are above 100 ppb with Mo ranging from 80 to 200 ppm, we argue that under reducing conditions, the concentration of dissolved Hg was limited and much lower than the maximum sequestration capability of organic matter and sulfide phases (for Hg), and that this explains the lack of correlation between Hg and Mo.

4.3.2. The V-δ^{202}Hg Proxy

Vanadium and Hg can be derived from seawater, terrestrial fractions, and magmatic activity (Bian, Chappaz, Schovsbo, & Sanei, 2022; Shen et al., 2020, 2023). A strongly negative V-δ^{202}Hg correlation in the late Cambrian samples—except for the most pronounced Hg anomalies ($n = 3$)—is found ($r_s = -0.87$, $p < 0.05$, $n = 11$; Figure 3b). Interestingly, this relationship is inversed for samples showing [V] > 1,000 ppm during loading event III. To interpret this negative correlation, we remark that the V concentrations range from 298 to 621 ppm, largely exceeding the upper crust level ($[V]_{crust} = 107$ ppm; McLennan, 2001), indicating those samples were deposited under reducing conditions. Given the long residence time of V (~91 ka) in seawater, which allows for sufficient mixing, it is unlikely that Hg originated solely from seawater, because of the lack of correlation between Mo and δ^{202}Hg (Figure S7 in Supporting Information S1). Bian, Chappaz, Schovsbo, and Sanei (2022) documented that V is mostly bound to sulfur atoms, probably buried in sulphurized organic matter. This is similar to the Hg structures and host phases in the Alum Shale. We thus propose the significant V-δ^{202}Hg correlation is attributed to (a) similar Hg and V sources and (b) reducing conditions that contributed to V enrichments and negative Hg MDF excursions. Although the reducing conditions were maintained, there is an inverse V-δ^{202}Hg correlation during the loading event III. Provided a stable supply of Hg from terrestrial fraction and seawater, as supported by CIA values (Figure S1i in Supporting Information S1) and Mo abundances (Figure S1d in Supporting Information S1), we argue that additional Hg sources (i.e., atmospheric Hg input) contributed to the high Hg concentrations we determined.

During the lower Tremadocian, V and δ^{202}Hg display a positive correlation. Considering that no distinct subaerial volcanic Hg inputs are identified, we infer that the coexistence of water upwelling and submarine volcanism account for the positive Hg MDF excursion and enrichments of V. Toward the end, this relationship becomes a negative relationship, similar to the late Cambrian, and consistent with a weakened upwelling of ocean water (Figure S1e in Supporting Information S1).

4.4. A Potential Global Impact

Numerous studies demonstrated the relative changes in Baltica's depositional environment are akin to the other continents including Avalonia, Laurentia, Gondwana, and Siberia (Figures 4f–4h). Constrained by a contemporaneous atmospheric-oceanic-biological model, we hypothesize on the global effects of volcanism on environmental and biological changes straddling the Cambro-Ordovician boundary.

During the Miaolingian, tectonic activity contributed to the formation of half-restricted continental margin basins and enhanced nutrient input through increased terrestrial erosion and upwelling of ocean water (Figure 4e). These conditions accelerated the biological productivity but also triggered adverse effects, such as the formation of sulfidic bottom water. The positive Hg and Mo correlation suggests that significant seawater inputs and sulfidic conditions contributed to Hg enrichments (Figure 3e). These conditions worsened and deteriorated the proper conditions to support life, resulting in the fact that increased extinction rate and reduced productivity drove carbon isotope excursion associated with the SPICE event (Figure 4f). During the Jiangshanian, the pronounced Hg anomalies suggest subaerial volcanism possibly associated with recurrent biological extinction (Figures 4b and 4g). This is followed by a decrease in seawater surface temperature, caused by intense terrestrial erosion from continents near the equator that enhanced atmospheric CO_2 consumption based on the modeled tectonic activity (Figures 1b and 4g). During the Stage 10, the negative Hg-Mo correlation indicates a continuous decrease in Hg input that is possibly ascribed to weakened volcanism.

During the early Tremadocian, a significant increase in magmatic activity occurred and was associated with water upwelling and associated elemental enrichments (e.g., Ag and Zn; Figures S2e–S2g and S4h in Supporting Information S1). These conditions may have increased water circulation and thus oxygenation, as well as brought significant amounts of nutrients, contributed to buffering the prior sulfidic conditions and promoted a thriving

highly diverse food web (Baross & Hoffman, 1985; Damer & Deamer, 2020). Moreover, the weakened terrestrial weathering could have decreased atmospheric CO_2 fixation and intense submarine magmatic activity could have promoted CO_2 release. These two factors may have been responsible for the contemporaneous global warming (Figure 4h).

5. Conclusions

Our study, for the first time, presents Hg systematics in sedimentary records across the entire Cambro-Ordovician boundary. A key finding is our interpretation of the Hg systematics: the most profound Furongian Hg anomalies displays slightly positive Δ^{199}Hg, Δ^{200}Hg, and Δ^{201}Hg values, and negative Δ^{204}Hg values, indicating subaerial Hg deposition, while the lower Tremadocian Hg perturbations are characterized by near-zero Hg MIFs values, suggesting an absence of photochemical processes. A second key finding is the two proposed new proxies (Hg-Mo and δ^{202}Hg-V relationships) that show that Hg fluxes were closely associated with environmental changes and volcanism. We suggest the gradually intense subaerial volcanism triggered the environmental deterioration of life from the late Miaolingian to mid Furongian and led to oceanic anoxia and biological extinctions. The Early Ordovician submarine volcanism was concurrent with significant water upwelling and contributed to the formation of nutrient-rich and less-reducing conditions on the shelf.

Data Availability Statement

The data set is available at the Open Science Framework (Bian, 2024).

Acknowledgments

We are grateful for the insightful comments that greatly improved this paper provided by Sarah Feakins (editor) and Jennifer Galloway (reviewer). We also acknowledge Naomi Nitschke and Emmanuel Tessier at the IPREM-CNRS. This work was funded by the National Natural Science Foundation of China (42225303), National Key Research and Development Program of China (2022YFF0800304), and PetroChina Limited Science and Technology Project (2023ZZ0203), as well as China Postdoctoral Science Foundation (2023M743888 and GZC20233109) awarded to L.B. and an ESF-EAR Grant 2051199 awarded to A.C.

References

Baross, J. A., & Hoffman, S. E. (1985). Submarine hydrothermal vents and associated gradient environments as sites for the origin and evolution of life. *Origins of Life and Evolution of the Biosphere*, *15*(4), 327–345. https://doi.org/10.1007/BF01808177

Bian, L. (2024). Improving mercury systematics with molybdenum and vanadium enrichments: New insights from the Cambrian-Ordovician boundary [Dataset]. *OSF*. https://doi.org/10.17605/OSF.IO/8XMTV

Bian, L., Chappaz, A., Schovsbo, N. H., Nielsen, A. T., & Sanei, H. (2022). High mercury enrichments in sediments from the Baltic continent across the late Cambrian: Controls and implications. *Chemical Geology*, *599*, 120846. https://doi.org/10.1016/j.chemgeo.2022

Bian, L., Chappaz, A., Schovsbo, N. H., & Sanei, H. (2022). A new vanadium species in black shales: Updated burial pathways and implications. *Geochimica et Cosmochimica Acta*, *338*, 1–10. https://doi.org/10.1016/j.gca.2022.09.035

Bian, L., Chappaz, A., Schovsbo, N. H., Wang, X., Zhao, W., & Sanei, H. (2023). A 20-million-year reconstruction to decipher the enigmatic Cambrian extinction–Ordovician biodiversification transition. *Earth and Planetary Science Letters*, *612*, 118170. https://doi.org/10.1016/j.epsl.2023.118170

Black, B. A., Karlstrom, L., & Mather, T. A. (2021). The life cycle of large igneous provinces. *Nature Reviews Earth & Environment*, *2*(12), 840–857. https://doi.org/10.1038/s43017-021-00221-4

Blum, J. D., & Johnson, M. W. (2017). Recent developments in mercury stable isotope analysis. *Reviews in Mineralogy and Geochemistry*, *82*(1), 733–757. https://doi.org/10.2138/rmg.2017

Blum, J. D., Sherman, L. S., & Johnson, M. W. (2014). Mercury isotopes in earth and environmental sciences. *Annual Review of Earth and Planetary Sciences*, *42*(1), 249–269. https://doi.org/10.1146/annurev-earth-050212-124107

Chappaz, A., Glass, J., & Lyons, T. W. (2018). Molybdenum. In W. M. White, W. H. Casey, B. Marty, & H. Yurimoto (Eds.), *Encyclopedia of Geochemistry* (Vol. 2, pp. 947–950). Springer International. https://doi.org/10.1007/978-3-319-39193-9_256-1

Chappaz, A., Lyons, T. W., Gregory, D. D., Reinhard, C. T., Gill, B. C., Li, C., & Large, R. R. (2014). Does pyrite act as an important host for molybdenum in modern and ancient euxinic sediments? *Geochimica et Cosmochimica Acta*, *126*, 112–122. https://doi.org/10.1016/j.gca.2013.10.028

Chen, C., Wang, J., Wang, Z., Peng, Y., Chen, X., Ma, X., et al. (2020). Variation of chemical index of alteration (CIA) in the Ediacaran Doushantuo Formation and its environmental implications. *Precambrian Research*, *347*, 105829. https://doi.org/10.1016/j.precamres.2020.105829

Damer, B., & Deamer, D. (2020). The hot spring hypothesis for an origin of life. *Astrobiology*, *20*(4), 429–452. https://doi.org/10.1089/ast.2019.2045

Demers, J. D., Blum, J. D., & Zak, D. R. (2013). Mercury isotopes in a forested ecosystem: Implications for air-surface exchange dynamics and the global mercury cycle. *Global Biogeochemical Cycles*, *27*(1), 222–238. https://doi.org/10.1002/gbc.20021

Fan, J. X., Shen, S. Z., Erwin, D. H., Sadler, P. M., MacLeod, N., Cheng, Q. M., et al. (2020). A high-resolution summary of Cambrian to Early Triassic marine invertebrate biodiversity. *Science*, *367*(6475), 272–277. https://doi.org/10.1126/science.aax4953

Fitzgerald, W. F., Lamborg, C. H., & Hammerschmidt, C. R. (2007). Marine biogeochemical cycling of mercury. *Chemical Reviews (Washington, DC, United States)*, *107*(2), 641–662. https://doi.org/10.1021/cr050353m

Gill, B. C., Lyons, T. W., Young, S. A., Kump, L. R., Knoll, A. H., & Saltzman, M. R. (2011). Geochemical evidence for widespread euxinia in the later Cambrian ocean. *Nature*, *469*(7328), 80–83. https://doi.org/10.1038/nature09700

Graham, A. M., Cameron-Burr, K. T., Hajic, H. A., Lee, C., Msekela, D., & Gilmour, C. C. (2017). Sulfurization of dissolved organic matter increases Hg–sulfide–dissolved organic matter bioavailability to a Hg-methylating bacterium. *Environmental Science & Technology*, *51*(16), 9080–9088. https://doi.org/10.1021/acs.est.7b02781

Grasby, S. E., Shen, W., Yin, R., Gleason, J. D., Blum, J. D., Lepak, R. F., et al. (2017). Isotopic signatures of mercury contamination in latest Permian oceans. *Geology*, *45*(1), 55–58. https://doi.org/10.1130/G38487.1

Grasby, S. E., Them II, T. R., Chen, Z., Yin, R., & Ardakani, O. H. (2019). Mercury as a proxy for volcanic emissions in the geologic record. *Earth-Science Reviews*, *196*, 102880. https://doi.org/10.1016/j.earscirev.2019.102880

Hagen, A. P., Jones, D. S., Tosca, N. J., Fike, D. A., & Pruss, S. B. (2022). Sedimentary mercury as a proxy for redox oscillations during the Cambrian SPICE event in western Newfoundland. *Canadian Journal of Earth Sciences*, *59*(8), 504–520. https://doi.org/10.1139/cjes-2021-0108

Harper, D. A., Cascales-Miñana, B., & Servais, T. (2020). Early palaeozoic diversifications and extinctions in the marine biosphere: A continuum of change. *Geological Magazine*, *157*(1), 5–21. https://doi.org/10.1017/S0016756819001298

Hauke, J., & Kossowski, T. (2011). Comparison of values of Pearson's and Spearman's correlation coefficients on the same sets of data. *Quaestiones Geographicae*, *30*(2), 87–93. https://doi.org/10.2478/v10117-011-0021-1

Hlohowskyj, S. R., Chappaz, A., & Dickson, A. J. (2021). Molybdenum as a paleoredox proxy: Past, present, and future. In T. Lyons, A. Turchyn, & C. Reinhard (Eds.), *Elements in geochemical tracers in Earth system science*. Cambridge University Press. https://doi.org/10.1017/9781108993777

Jones, M. T., & Gislason, S. R. (2008). Rapid releases of metal salts and nutrients following the deposition of volcanic ash into aqueous environments. *Geochimica et Cosmochimica Acta*, *72*(15), 3661–3680. https://doi.org/10.1016/j.gca.2008.05.030

Lindström, S., Sanei, H., Van De Schootbrugge, B., Pedersen, G. K., Lesher, C. E., Tegner, C., et al. (2019). Volcanic mercury and mutagenesis in land plants during the end-Triassic mass extinction. *Science Advances*, *5*(10), eaaw4018. https://doi.org/10.1126/sciadv.aaw4018

Longman, J., Mills, B. J., Manners, H. R., Gernon, T. M., & Palmer, M. R. (2021). Late Ordovician climate change and extinctions driven by elevated volcanic nutrient supply. *Nature Geoscience*, *14*(12), 924–929. https://doi.org/10.1038/s41561-021-00855-5

Mason, R. P., & Sheu, G. R. (2002). Role of the ocean in the global mercury cycle. *Global Biogeochemical Cycles*, *16*(4), 1–13. https://doi.org/10.1029/2001GB001440

McArthur, J. M., Howarth, R. J., Shields, G. A., & Zhou, Y. (2020). Strontium isotope stratigraphy. In F. M. Gradstein, J. G. Ogg, M. D. Schmitz, & G. M. Ogg (Eds.), *Geologic time scale 2020* (pp. 211–238). Elsevier. https://doi.org/10.1016/B978-0-12-824360-2.00007-3

McLennan, S. M. (2001). Relationships between the trace element composition of sedimentary rocks and upper continental crust. *Geochemistry, Geophysics, Geosystems*, *2*(4). https://doi.org/10.1029/2000GC000109

McLennan, S. M., Hemming, S., McDaniel, D. K., & Hanson, G. N. (1993). Geochemical approaches to sedimentation, provenance, and tectonics. In M. J. Johnsson & A. Basu (Eds.), *Processes controlling the composition of clastic sediments* (Vol. 284, pp. 21–41). Geological Society of America-Special Papers. https://doi.org/10.1130/SPE284-p21

Meixnerová, J., Blum, J. D., Johnson, M. W., Stüeken, E. E., Kipp, M. A., Anbar, A. D., & Buick, R. (2021). Mercury abundance and isotopic composition indicate subaerial volcanism prior to the end-Archean "whiff" of oxygen. *Proceedings of the National Academy of Sciences of the United States of America*, *118*(33), e2107511118. https://doi.org/10.1073/pnas.2107511118

Miller, C. A., Peucker-Ehrenbrink, B., Walker, B. D., & Marcantonio, F. (2011). Re-assessing the surface cycling of molybdenum and rhenium. *Geochimica et Cosmochimica Acta*, *75*(22), 7146–7179. https://doi.org/10.1016/j.gca.2011.09.005

Nesbitt, H., & Young, G. M. (1982). Early Proterozoic climates and plate motions inferred from major element chemistry of lutites. *Nature*, *299*(5885), 715–717. https://doi.org/10.1038/299715a0

Nielsen, A. T., & Schovsbo, N. H. (2015). The regressive early-mid Cambrian "Hawke Bay Event" in Baltoscandia: Epeirogenic uplift in concert with eustasy. *Earth-Science Reviews*, *151*, 288–350. https://doi.org/10.1016/j.earscirev.2015.09.012

Rickard, D., & Morse, J. W. (2005). Acid volatile sulfide (AVS). *Marine Chemistry*, *97*(3–4), 141–197. https://doi.org/10.1016/j.marchem.2005.08.004

Saltzman, M. R., Edwards, C. T., Adrain, J. M., & Westrop, S. R. (2015). Persistent oceanic anoxia and elevated extinction rates separate the Cambrian and Ordovician radiations. *Geology*, *43*(9), 807–810. https://doi.org/10.1130/G36814.1

Sanei, H., Grasby, S. E., & Beauchamp, B. (2012). Latest Permian mercury anomalies. *Geology*, *40*(1), 63–66. https://doi.org/10.1130/G32596.1

Selin, N. E. (2009). Global biogeochemical cycling of mercury: A review. *Annual Review of Environment and Resources*, *34*(1), 43–63. https://doi.org/10.1146/annurev.environ.051308.084314

Servais, T., & Harper, D. A. (2018). The great Ordovician biodiversification event (GOBE): Definition, concept and duration. *Lethaia*, *51*(2), 151–164. https://doi.org/10.1111/let.12259

Shen, J., Algeo, T. J., Planavsky, N. J., Yu, J., Feng, Q., Song, H., et al. (2019). Mercury enrichments provide evidence of Early Triassic volcanism following the end-Permian mass extinction. *Earth-Science Reviews*, *195*, 191–212. https://doi.org/10.1016/j.earscirev.2019.05.010

Shen, J., Chen, J., Yu, J., Algeo, T. J., Smith, R. M., Botha, J., et al. (2023). Mercury evidence from southern Pangea terrestrial sections for end-Permian global volcanic effects. *Nature Communications*, *14*(1), 6. https://doi.org/10.1038/s41467-022-35272-8

Shen, J., Feng, Q., Algeo, T. J., Liu, J., Zhou, C., Wei, W., et al. (2020). Sedimentary host phases of mercury (Hg) and implications for use of Hg as a volcanic proxy. *Earth and Planetary Science Letters*, *543*, 116333. https://doi.org/10.1016/j.epsl.2020.116333

Shen, J., Yin, R., Algeo, T. J., Svensen, H. H., & Schoepfer, S. D. (2022). Mercury evidence for combustion of organic-rich sediments during the end-Triassic crisis. *Nature Communications*, *13*(1), 1307. https://doi.org/10.1038/s41467-022-28891-8

Skyllberg, U., & Drott, A. (2010). Competition between disordered iron sulfide and natural organic matter associated thiols for mercury (II)-An EXAFS study. *Environmental Science & Technology*, *44*(4), 1254–1259. https://doi.org/10.1021/es902091w

Torsvik, T. H., & Cocks, L. R. M. (2013). New global palaeogeographical reconstructions for the early Palaeozoic and their generation. *Geological Society Memoirs*, *38*(1), 5–24. https://doi.org/10.1144/M38.2

Wallace, G. T., Jr. (1982). The association of copper, mercury and lead with surface-active organic matter in coastal seawater. *Marine Chemistry*, *11*(4), 379–394. https://doi.org/10.1016/0304-4203(82)90032-9

Wolfenden, S., Charnock, J. M., Hilton, J., Livens, F. R., & Vaughan, D. J. (2005). Sulfide species as a sink for mercury in lake sediments. *Environmental Science & Technology*, *39*(17), 6644–6648. https://doi.org/10.1021/es048874z

Zerkle, A. L., Yin, R., Chen, C., Li, X., Izon, G. J., & Grasby, S. E. (2020). Anomalous fractionation of mercury isotopes in the Late Archean atmosphere. *Nature Communications*, *11*(1), 1709. https://doi.org/10.1038/s41467-020-15495-3

References From the Supporting Information

Andréasson, P. G., & Albrecht, L. (1995). Derivation of 500 Ma eclogites from the passive margin of Baltica and a note on the tectonometamorphic heterogeneity of eclogite-bearing crust. *Geological Magazine*, *132*(6), 729–738. https://doi.org/10.1017/S001675680001894X

Alexeiev, D. V., Kröner, A., Kovach, V. P., Tretyakov, A. A., Rojas-Agramonte, Y., Degtyarev, K. E., et al. (2019). Evolution of Cambrian and early Ordovician arcs in the Kyrgyz North Tianshan: Insights from U-Pb zircon ages and geochemical data. *Gondwana Research*, *66*, 93–115. https://doi.org/10.1016/j.gr.2018.09.005

Algeo, T. J., Chen, Z., Fraiser, M. L., & Twitchett, R. J. (2011). Terrestrial–marine teleconnections in the collapse and rebuilding of Early Triassic marine ecosystems. *Palaeogeography, Palaeoclimatology, Palaeoecology*, *308*(1–2), 1–11. https://doi.org/10.1016/j.palaeo.2011.01.011

Andersson, A., Dahlman, B., Gee, D. G., & Snall, S. (1985). The Scandinavian alum shales. In *Sveriges geologiska undersökning. Serie Ca: Avhandlingar och uppsatser I* (Vol. A4, p. 35). Retrieved from https://paleoarchive.com/literature/Anderssonetal1985-ScandinavianAlumShales.pdf

Becerra-Castro, C., Kidd, P., Kuffner, M., Prieto-Fernández, Á., Hann, S., Monterroso, C., et al. (2013). Bacterially induced weathering of ultramafic rock and its implications for phytoextraction. *Applied and Environmental Microbiology*, *79*(17), 5094–5103. https://doi.org/10.1128/AEM.00402-13

Bian, L., Schovsbo, N. H., Chappaz, A., Zheng, X., Nielsen, A. T., Ulrich, T., et al. (2021). Molybdenum-uranium-vanadium geochemistry in the lower paleozoic alum shale of Scandinavia: Implications for vanadium exploration. *International Journal of Coal Geology*, *239*, 103730. https://doi.org/10.1016/j.coal.2021.103730

Bloom, N. S., Preus, E., Katon, J., & Hiltner, M. (2003). Selective extractions to assess the biogeochemically relevant fractionation of inorganic mercury in sediments and soils. *Analytica Chimica Acta*, *479*(2), 233–248. https://doi.org/10.1016/S0003-2670(02)01550-7

Brocza, F. M., Biester, H., Richard, J. H., Kraemer, S. M., & Wiederhold, J. G. (2019). Mercury isotope fractionation in the subsurface of a Hg (II) chloride-contaminated industrial legacy site. *Environmental Science & Technology*, *53*(13), 7296–7305. https://doi.org/10.1021/acs.est.9b00619

Cramer, B. D., & Jarvis, I. (2020). Carbon isotope stratigraphy, Strontium isotope stratigraphy. In F. M. Gradstein, J. G. Ogg, M. D. Schmitz, & G. M. Ogg (Eds.), *Geologic time Scale 2020* (pp. 309–343). Elsevier. https://doi.org/10.1016/B978-0-12-824360-2.00011-5

Foden, J., Elburg, M., Turner, S., Clark, C., Blades, M. L., Cox, G., et al. (2020). Cambro-Ordovician magmatism in the Delamerian orogeny: Implications for tectonic development of the southern Gondwanan margin. *Gondwana Research*, *81*, 490–521. https://doi.org/10.1016/j.gr.2019.12.006

García-Arias, M., Díez-Montes, A., Villaseca, C., & Blanco-Quintero, I. F. (2018). The Cambro-Ordovician Ollo de Sapo magmatism in the Iberian Massif and its Variscan evolution: A review. *Earth-Science Reviews*, *176*, 345–372. https://doi.org/10.1016/j.earscirev.2017.11.004

Gee, D. G. (1987). The Scandinavian alum shales-Mid Cambrian to Tremadoc deposition in response to early Caledonian subduction. *Norsk Geologisk Tidsskrift*, *67*, 233–235.

Gill, B. C., Dahl, T. W., Hammarlund, E. U., LeRoy, M. A., Gordon, G. W., Canfield, D. E., et al. (2021). Redox dynamics of later Cambrian oceans. *Palaeogeography, Palaeoclimatology, Palaeoecology*, *581*, 110623. https://doi.org/10.1016/j.palaeo.2021.110623

Goldberg, S. L., Present, T. M., Finnegan, S., & Bergmann, K. D. (2021). A high-resolution record of early Paleozoic climate. *Proceedings of the National Academy of Sciences*, *118*(6), e2013083118. https://doi.org/10.1073/pnas.2013083118

Grigg, A. R., Kretzschmar, R., Gilli, R. S., & Wiederhold, J. G. (2018). Mercury isotope signatures of digests and sequential extracts from industrially contaminated soils and sediments. *Science of the Total Environment*, *636*, 1344–1354. https://doi.org/10.1016/j.scitotenv.2018.04.261

Guédron, S., Amouroux, D., Sabatier, P., Desplanque, C., Develle, A. L., Barre, J., et al. (2016). A hundred year record of industrial and urban development in French Alps combining Hg accumulation rates and isotope composition in sediment archives from Lake Luitel. *Chemical Geology*, *431*, 10–19. https://doi.org/10.1016/j.chemgeo.2016.03.016

Kröner, A., Alexeiev, D. V., Rojas-Agramonte, Y., Hegner, E., Wong, J., Xia, X., et al. (2013). Mesoproterozoic (Grenville-age) terranes in the Kyrgyz North Tianshan: Zircon ages and Nd–Hf isotopic constraints on the origin and evolution of basement blocks in the southern Central Asian Orogen. *Gondwana Research*, *23*(1), 272–295. https://doi.org/10.1016/j.gr.2012.05.004

Lassen, A., & Thybo, H. (2012). Neoproterozoic and Palaeozoic evolution of SW Scandinavia based on integrated seismic interpretation. *Precambrian Research*, *204*, 75–104. https://doi.org/10.1016/j.precamres.2012.01.008

Monperrus, M., Rodriguez Gonzalez, P., Amouroux, D., Garcia Alonso, J. I., & Donard, O. F. (2008). Evaluating the potential and limitations of double-spiking species-specific isotope dilution analysis for the accurate quantification of mercury species in different environmental matrices. *Analytical and Bioanalytical Chemistry*, *390*(2), 655–666. https://doi.org/10.1007/s00216-007-1598-z

Montero, P., Bea, F., González-Lodeiro, F., Talavera, C., & Whitehouse, M. J. (2007). Zircon ages of the metavolcanic rocks and metagranites of the Ollo de Sapo Domain in central Spain: Implications for the Neoproterozoic to early Palaeozoic evolution of Iberia. *Geological Magazine*, *144*(6), 963–976. https://doi.org/10.1017/S0016756807003858

Montero, P., Talavera, C., Bea, F., Lodeiro, F. G., & Whitehouse, M. J. (2009). Zircon geochronology of the Ollo de Sapo formation and the age of the Cambro-Ordovician rifting in Iberia. *The Journal of Geology*, *117*(2), 174–191. https://doi.org/10.1086/595017

Nielsen, A. T., & Schovsbo, N. H. (2007). Cambrian to basal Ordovician lithostratigraphy in southern Scandinavia. *Bulletin of the Geological Society of Denmark*, *53*, 47–92. https://doi.org/10.37570/bgsd-2006-53-04

Ofili, S., Soesoo, A., Panova, E. G., Hints, R., Hade, S., & Ainsaar, L. (2022). Geochemical reconstruction of the provenance, tectonic setting and paleoweathering of lower paleozoic black shales from northern Europe. *Minerals*, *12*(5), 602. https://doi.org/10.3390/min12050602

Parker, A. (1970). An index of weathering for silicate rocks. *Geological Magazine*, *107*(6), 501–504. https://doi.org/10.1017/S0016756800058581

Penman, D. E., Rugenstein, J. K. C., Ibarra, D. E., & Winnick, M. J. (2020). Silicate weathering as a feedback and forcing in Earth's climate and carbon cycle. *Earth-Science Reviews*, *209*, 103298. https://doi.org/10.1016/j.earscirev.2020.103298

Pruss, S. B., Jones, D. S., Fike, D. A., Tosca, N. J., & Wignall, P. B. (2019). Marine anoxia and sedimentary mercury enrichments during the Late Cambrian SPICE event in northern Scotland. *Geology*, *47*(5), 475–478. https://doi.org/10.1130/G45871.1

Putiš, M., Sergeev, S., Ondrejka, M., Larionov, A., Siman, P., Spisiak, J., et al. (2008). Cambrian-Ordovician metaigneous rocks associated with Cadomian fragments in the West-Carpathian basement dated by SHRIMP on zircons: A record from the Gondwana active margin setting. *Geological Carpathica-Bratislava*, *59*, 3–18.

Rasmussen, C. M. Ø., Kröger, B., Nielsen, M. L., & Colmenar, J. (2019). Cascading trend of Early Paleozoic marine radiations paused by Late Ordovician extinctions. *Proceedings of the National Academy of Sciences of the United States of America*, *116*(15), 7207–7213. https://doi.org/10.1073/pnas.1821123116

Rico, K. I., Sheldon, N. D., Gallagher, T. M., & Chappaz, A. (2019). Redox chemistry and molybdenum burial in a Mesoproterozoic Lake. *Geophysical Research Letters*, *46*(11), 5871–5878. https://doi.org/10.1029/2019GL083316

Root, D., & Corfu, F. (2012). U–Pb geochronology of two discrete Ordovician high-pressure metamorphic events in the Seve Nappe Complex, Scandinavian Caledonides. *Contributions to Mineralogy and Petrology*, *163*(5), 769–788. https://doi.org/10.1007/s00410-011-0698-0

Saltzman, M. R., Young, S. A., Kump, L. R., Gill, B. C., Lyons, T. W., & Runnegar, B. (2011). Pulse of atmospheric oxygen during the late Cambrian. *Proceedings of the National Academy of Sciences of the United States of America*, *108*(10), 3876–3881. https://doi.org/10.1073/pnas.1011836108

Schovsbo, N. H., Nielsen, A. T., & Gautier, D. L. (2014). The Lower Palaeozoic shale gas play in Denmark. *GEUS Bulletin*, *31*, 19–22. https://doi.org/10.34194/geusb.v31.4640

Sweere, T., van den Boorn, S., Dickson, A. J., & Reichart, G. J. (2016). Definition of new trace-metal proxies for the controls on organic matter enrichment in marine sediments based on Mn, Co, Mo and Cd concentrations. *Chemical Geology*, *441*, 235–245. https://doi.org/10.1016/j.chemgeo.2016.08.028

Talavera, C., Montero, P., Bea, F., González Lodeiro, F., & Whitehouse, M. (2013). U–Pb zircon geochronology of the Cambro-Ordovician metagranites and metavolcanic rocks of central and NW Iberia. *International Journal of Earth Sciences*, *102*, 1–23. https://doi.org/10.1007/s00531-012-0788-x

Tchaptchet, T. W., Tematio, P., Guimapi, T. N., Happi, E., Tiomo, I., & Momo, N. M. (2021). Morphological, mineral and geochemical characterization of soil profiles in Meïganga as tools for rock weathering intensity and trend evaluation and residual ore deposit prospection in the mineralized domain of central Cameroon. In T. Aïfa (Ed.), *Mineralization and sustainable development in the West African Craton: From field observations to modelling*. Geological Society, London, Special Publications. https://doi.org/10.1144/SP502-2019-84

Thickpenny, A. (1987). Palaeo-oceanography and depositional environment of the Scandinavian Alum Shales: Sedimentological and geochemical evidence. In J. K. Leggett & G. G. Zuffa (Eds.), *Marine clastic sedimentology: Concepts and case studies* (pp. 156–171). Springer. https://doi.org/10.1007/978-94-009-3241-8_8

Vozárová, A., Šarinová, K., Larionov, A., Presnyakov, S., & Sergeev, S. (2010). Late Cambrian/Ordovician magmatic arc type volcanism in the southern Gemericum basement, western Carpathians, Slovakia: U–Pb (SHRIMP) data from zircons. *International Journal of Earth Sciences*, *99*(S1), 17–37. https://doi.org/10.1007/s00531-009-0454-0

Vozárová, A., Rodionov, N., Šarinová, K., & Presnyakov, S. (2017). New zircon ages on the Cambrian–Ordovician volcanism of the southern Gemericum basement (western Carpathians, Slovakia): SHRIMP dating, geochemistry and provenance. *International Journal of Earth Sciences*, *106*(6), 2147–2170. https://doi.org/10.1007/s00531-016-1420-2

Wiederhold, J. G., Skyllberg, U., Drott, A., Jiskra, M., Jonsson, S., Bjorn, E., et al. (2015). Mercury isotope signatures in contaminated sediments as a tracer for local industrial pollution sources. *Environmental Science & Technology*, *49*(1), 177–185. https://doi.org/10.1021/es5044358

Zheng, X., Schovsbo, N. H., Bian, L., Luo, Q., Zhong, N., Rudra, A., et al. (2021). Alteration of organic macerals by uranium irradiation in lower Paleozoic marine shales. *International Journal of Coal Geology*, *239*, 103713. https://doi.org/10.1016/j.coal.2021.103713

Zheng, X., Schovsbo, N. H., Bian, L., Rudra, A., & Sanei, H. (2023). Organic geochemical and petrographic characteristics of the Cambrian-Ordovician organic-rich marine shales in Scandinavia. *Petroleum Science*, *20*(5), 2637–2647. https://doi.org/10.1016/j.petsci.2023.04.011

Zhu, D., Zhao, Z., Niu, Y., Dilek, Y., Wang, Q., Ji, W., et al. (2012). Cambrian bimodal volcanism in the Lhasa Terrane, southern Tibet: Record of an early paleozoic Andean-type magmatic arc in the Australian proto-Tethyan margin. *Chemical Geology*, *328*, 290–308. https://doi.org/10.1016/j.chemgeo.2011.12.024